HHS Public Access

Author manuscript

Nat Biomed Eng. Author manuscript; available in PMC 2019 August 25.

Published in final edited form as:

Nat Biomed Eng. 2019 August ; 3(8): 621–631. doi:10.1038/s41551-019-0350-2.

A resistance-sensing mechanical injector for the precise delivery of liquids to target tissue

Girish D. Chitnis[1,2], **Mohan K. S. Verma**[*,1,2], **Julien Lamazouade**[*,1,2], **Miguel Gonzalez-Andrades**[6,7], **Kisuk Yang**[1,2,3,4,5], **Ali Dergham**[1,2], **Peter Anthony Jones**[1,2], **Benjamin E. Mead**[1,2,3,4,5], **Andrea Cruzat**[6], **Zhixiang Tong**[1,2], **Keir Martyn**[1,2], **Aniruddh Solanki**[1,2], **Natalie Landon-Brace**[1,2], **Jeffrey M. Karp**[✉,1,2,4,5]

[1]Engineering in Medicine, Department of Medicine, Center for Regenerative Therapeutics, Brigham and Women's Hospital, Harvard Medical School, Massachusetts, USA

[2]Harvard-MIT Division of Health Sciences and Technology, MIT, Cambridge, Massachusetts, USA

[3]Koch Institute for Integrative Cancer Research, MIT, Cambridge, Massachusetts, USA

[4]Broad Institute of Harvard and MIT, Cambridge, Massachusetts, USA

[5]Harvard Stem Cell Institute, 1350 Massachusetts Avenue, Cambridge, Massachusetts 02138, USA

[6]Schepens Eye Research Institute and Massachusetts Eye and Ear, Department of Ophthalmology, Harvard Medical School, Boston, Massachusetts, USA.

[7]Maimonides Biomedical Research Institute of Cordoba (IMIBIC), Department of Ophthalmology, Reina Sofia University Hospital and University of Cordoba, Cordoba, Spain.

Abstract

The precision of the delivery of therapeutics to the desired injection site by using syringes and hollow needles typically depends on the operator. Here, we introduce a highly sensitive, completely mechanical and cost-effective injector for targeting tissue reliably and precisely. As the operator pushes on the syringe plunger, the injector senses the loss-of-resistance on encountering a softer tissue or a cavity, stops advancing the needle, and delivers the payload. We demonstrate that the injector can reliably deliver liquids to the suprachoroidal space — a challenging injection site that provides access to the back of the eye — for a wide range of eye sizes, scleral thicknesses and

✉Corresponding author.

*Equally contributing second authors

Author contributions

G.C. and M.K.S.V. conceptualized the principle of *i*2T2. G.C., M.K.S.V. and J.L. were responsible for study design guided by J.M.K.. G.C. and J.L. developed the analytical model, improved design, and performed detailed experimental studies with focus on ocular applications. G.C., M.G.A., A.C. and J.L. designed and performed in vivo experiments. B.E.M., A.S., N.L.B., Z.T., K.M., and K.Y. provided experimental support for the experiments with cell-injections in SCS. G.C., M.K.S.V., and A.D. tested the device for applications other than eye. G.C. and J.L. were responsible for conceptual drawings and data representation. B.E.M. captured all the photographs under supervision of G.C. and J.L. G.C. wrote the manuscript with constructive feedback and editing from J.M.K., J.L., B.E.M., and P.A.J.

Competing interests

The authors declare no competing interests.

intraocular pressures, and to target sites relevant for epidural injections, subcutaneous injections and intraperitoneal access. The design of this simple and effective injector can be adapted for a broad variety of clinical applications.

Misdirected injection of therapeutic and diagnostic agents can severely compromise efficacy and lead to serious complications[1–5]. The century-old method of infusing fluids into the body with a syringe and a hollow needle can be improved with a system that is less reliant on the operator's skills and enables automated access to the target site despite anatomical variations. Insertion of sharp tools into a target space is also common for biopsy, aspirating fluids, and laparoscopic surgery, which face the same challenge. While these procedures are ubiquitous and have enabled multiple life-saving treatments, improper insertion or positioning of needles, catheters, and trocars can cause mechanical injury to adjacent tissues, or misdirected drug infusion, and often require repeated attempts to achieve correct placement. Live imaging/sensing systems[6] like fluoroscopy[7], CT scan[8] or ultrasound[9,10] are available at an added cost, time, and resources, however they often do not have the sufficient resolution to perfect needle placement or are not preferred by physicians, or simply can't be used (e.g. in emergent situations). Current techniques for accessing specific regions of the body with needles typically involve blind insertion where the physician or nurse relies entirely on superficial anatomical landmarks, experience, fluid return through the instrument, and ta ctile feedback from change in resistance to pierce through tissue layers. Current approaches require the operator to quickly sense and stop advancing the needle once in the targeted tissue, cavity, or potential space. Depending on the application, such feedback may be absent or not sensitive enough to be detected by the operator. Where feedback is detectable, final placement of the needle is highly sensitive to the speed of insertion and the reaction time of the operator.

Devices like the Veress needle[11], spring-loaded trocars, and mechanisms to stop[12], retract[13] or sense the position[14,15] of the needle, attempt to limit the injury caused to the neighboring tissue during pneumoperitoneum or epidural injection. Data supporting the effectiveness of these devices in avoiding the damage remains weak [16–18]. Furthermore, these mechanisms can't be miniaturized cost-effectively to adapt for smaller needle sizes. A force-sensing microneedle[19] has been developed for retinal vein cannulation which demands complex sensing devices and relies on the operator to arrest the needle motion. Here we introduce a highly sensitive, completely mechanical, and cost-effective device, an intelligent-injector for tissue-targeting (*i*2T2), that senses the loss-of-resistance, stops advancing the needle automatically, and delivers the payload, while the operator simply pushes on the syringe plunger in one continuous motion to enable all three actions. Since the device is designed based on the physics underlying the general process of needle insertion, it can be adapted for a large range of medical applications. An analytical model developed for the design of this device enabled us to customize parameters for the *i*2T2 to ensure successful tissue-targeted injection to access multiple cavities and tissues ranging from large peritoneal cavity under layers of skin, fat, and muscles, to the micro-thin suprachoroidal space below the sclera. Amongst multiple targets, suprachoroidal space (SCS) is one of the most unforgiving sites. The SCS is a relatively new site for drug delivery that has the potential of allowing instantaneous delivery to the back of the eye[20–30]. Direct injection near the diseased site

minimizes dosage necessary for the therapeutic effect and minimizes systemic toxicity. SCS injections involve the insertion of a needle through the sclera to access the SCS and deliver drugs to the back of the eye, without penetrating the underlying choroid and retina. The thin tissue layers (healthy human sclera: 0.7–1.1 mm, choroid: 0.18–0.24 mm, retina: 0.22–0.34 mm)[34] make it difficult to consistently access the SCS without overshooting into the vitreous space. Additionally, the sclera is 10-times stiffer than the choroid, and 200-times stiffer than the retina[34], making it even more challenging to pierce the sclera without puncturing through the choroid and retina. This application demands engineering precision and miniaturization with limited room for error. While it is simpler to implement *i*2T2 for applications involving thicker tissue structures and larger cavities, we selected drug delivery into the SCS as a gateway model to first validate functionality and safety of the *i*2T2. Specifically, our thinking was that success of *i*2T2 with SCS delivery would open the door to many other applications. We recognize that multiple specialized techniques and devices[22,35] have been developed to access this space. However, none of those techniques can be translated to other medical applications. Following a robust proof of concept with SCS delivery, we demonstrate that the *i*2T2 can target the site of interest for epidural injections, subcutaneous injections, and intraperitoneal access. Overall, the *i*2T2 overcomes the limitations of standard fixed length needles by automating the loss-of-resistance technique to enable safer and easier access to target sites with applications ranging from SCS delivery to epidural injection.

Results:

System design and approach

The device consists of a standard hypodermic needle that senses the loss of resistance to fluid flow as it advances through the tissue and arrests the motion automatically as the needle tip enters the tissue that offers lower resistance. Specifically, a sliding hypodermic needle penetrates through the outer tissue layer, automatically stops at the interface of two tissue layers, and delivers the contents of the syringe into the targeted space as the user pushes the plunger in a single continuous motion (fig. 1a-e). The needle is mounted on a sliding support (termed a ‘needle-plunger’), to enable movement of the needle along the axis of the syringe barrel. The first step of delivery with the *i*2T2 is insertion of needle tip into the tissue at a shallow depth, just enough to block fluid flow through the needle (stage I- ‘pre-insertion’). The syringe barrel prevents excessive penetration of the needle into the tissue, and the needle-plunger-seat prevents the backward motion of the needle (fig. 1b). As the internal fluid is pressurized by pushing on the plunger, the driving forces acting on the needle overcome the opposing forces and advance the needle deeper into the tissue, while the barrel remains stationary (stage II: ‘tissue penetration’) (fig. 1c). When the needle tip enters the target space (fig 1d), fluid starts exiting immediately (fig. 1e) to drop the internal pressure and effectively lower the driving force below the opposing force and arrest the needle at the interface. Hence fluid is delivered in the targeted tissue of lower resistance as the operator continues to move the pushing plunger (stage III: ‘targeted delivery’). This automatic stop is accompanied by tactile feedback due to a sudden drop in pushing force (fig. 1f). and visual feedback through the now motionless needle-plunger to assure the user of entry into the target cavity.

A functional *i*2T2 is realized with minimal modifications to the standard syringe-needle system as a stand-alone device (fig. 1g-h), as a modular system that works with a range of syringes (fig. 1i-k), within the insulin injector that has a different grip (fig. 1l), and with a spring-loaded plunger (fig. 1m-n).

*i*2T2 for suprachoroidal injections

A number of design criteria were considered while selecting a *i*2T2 for SCS delivery, including a range of possible variations in device design, needle size, syringe size, and flow rate. Typically, in the clinic, syringes are either pre-filled or loaded with a larger-bore needle for quick filling. Hence, a system where an auto-stop component can be connected after drug loading, i.e. detachable *i*2T2 (fig. 1m), was chosen for the SCS injection. SCS is present surrounding almost the entire posterior section of the eye. We used the anterior portion of the sclera for needle insertion which allows easy access to SCS without any surgical procedure. By inserting the needle at a set distance from the limbus for a given species, one can ensure that the needle is well positioned to enter the SCS.

Successful delivery with *i*2T2 requires that the injector performs as intended in all the three stages. With a minimal human scleral thickness[34] in mind, we limited the pre-insertion depth to 500 μm. If inserted at an angle other than perpendicular, one can bury the needle deeper without piercing through the sclera. For example, a 30 G needle with the standard bevel (angle: 12º, length: 1.45 mm), inserted at an angle smaller than 30º to the surface, satisfies these criteria. The driving force (which enable forward motion of needle) and opposing force (which oppose the needle motion) play a critical role in stages II and III to control the needle's motion and its automatic stop at the loss of resistance. (supplementary information S1). Commonly used ocular needles (27G, 30G, and 33G) are able to overcome the opposing force with a sufficient driving force in stage-II (fig. 2a) as the needle moves through sclera at a range of speeds (10–50 mm/min), indicating successful tissue insertion. Similarly, with water as the fluid, the driving force for the same needles is lower than the opposing friction at multiple speeds (10, 30, and 50 mm/min) of the pushing plunger (fig. 2b), indicating that the *i*2T2 will function as designed for SCS injections. We picked a 30G needle for the device because of its wide-spread use for intravitreal injections.

Syringe size and speed of injection are determined with help of an experimentally verified analytical model (supplementary information S1) that predicts maximum allowable fluid flow rate (i.e. speed of injection) for a given set of parameters (fluid viscosity, plunger-friction, syringe barrel diameter, and needle size). Due to the lack of approved formulations for SCS delivery, the design is based on formulations used for intravitreal injections, which typically have a viscosity like water (1 cP). Figure 2c plots the maximum flow rates that allow for automatic stop in stage III for aqueous formulations (viscosity = 1 cP) for multiple needle sizes and syringe sizes based on the analytical model. Clearly, a 1-ml syringe allows for a large range of fluid flow rates (0.18 ml/min to 2.2 ml/min) and it can comfortably deliver 50–200 μl of fluid, a typical volume for SCS injections. In other words, this allows a clinician 33 seconds to inject 100 μl fluid into the SCS. A typical intravitreal injection (time of injection: ~15s, excluding injection site preparation time) fits well within this window of injection-speed with sufficient room for error.

*i*2T2 enables targeted delivery into the SCS

The *i*2T2 was tested for its ability to deliver drug into SCS by injecting a model dye formulation (histology marking dye or X-ray contrast agent) into *ex vivo* bovine eyes (fig. 2d). Histology slides clearly show the green dye spread out across the SCS (fig. 2e-f). The angle of the needle track visible in the sclera is representative of the initial insertion angle. The 3-dimensional images obtained with X-ray microtomography (fig. 2g) show that a single injection spreads the dose along the periphery to cover a large portion of the SCS immediately after injection. These observations confirm targeted delivery into the SCS with *i*2T2. As a negative control, a standard needle was pierced through all the tissue layers to reach the vitreous. We did not observe the presence of contrast agent in the SCS and all the payload was delivered into the vitreous which is observed as a bright 'spot' within the vitreous at a distance from the retina (supplementary fig. S3). We also performed serial sections along the path of the needle to verify the needle traveled through the sclera and did not pierce the retinal pigment epithelium (RPE) or other inner tissue layers. (supplementary fig. S4).

Variation in eye anatomy does not affect delivery with the *i*2T2

We performed SCS injections with *i*2T2 in multiple eyes (*ex vivo*) with a wide range of scleral thickness, intraocular pressure, and eye sizes. The location of the delivery (observed with microCT, supplementary fig. S3) and total coverage of SCS with a single injection (fig. 3a-b) is not affected by scleral thickness at the site of injection or intraocular pressure. While the eye size does not affect location of delivery (fig. 3c-e); it increases relative SCS coverage for smaller eyes (bovine, porcine, and rabbit) when same fluid-volume is administered (fig. 3f). Similarly, increasing the volume increases the SCS coverage (fig. 3g).

*i*2T2 can deliver a payload to the retina and nearby inner tissue layers through diffusion

We used Ultravist™ (active molecule: Iopromide, M.W.: 791) contrast agent as a surrogate for a small molecule drug to visualize diffusion through multiple tissue layers (choroid, retinal pigment epithelium, and retina) by microCT. A bovine eye imaged at multiple time points after SCS injection (fig. 4a) shows that while SCS coverage was maintained, the agent starts diffusing within minutes across both inner and outer tissue layers. Immediately after injection, the dye had spread along the periphery yet was confined to a thin layer as indicated by a sharp spike in brightness (fig. 4b). This confined dye diffuses to the surrounding tissue (fig. 4c) increasing in the vitreous near the retina as indicated by increasing area under the curve (fig. 4d).

*i*2T2 can deliver micro-particles and live cells throughout the entire SCS for cell therapy

Drug delivery to the posterior segment of the eye through SCS is limited by the clearance rate of drugs through the choroidal vasculature. Sustained drug delivery using polymeric particles or cells can have more lasting effects. The trophic effect of certain cell types, such as mesenchymal stem cells (MSCs)[39] and human umbilical cord cells[40], has been shown to be effective in limiting ocular tissue degeneration for multiple diseases. With the *i*2T2, micro-particles and cells can be distributed within SCS to be in close proximity of retina and RPE. We delivered polymer particles (Polybeads®, 0.20 μm) and tagged (DiD) MSCs into

the SCS of bovine eyes (*ex vivo*). Particle delivery into SCS was confirmed using histology (fig. 5b) compared to a control injected with PBS (fig. 5a). The presence of tagged cells below the sclera was confirmed with intravital microscopy (fig. 5c-e). In a separate experiment, tagged (CellTrace™ Violet) MSCs were injected into the SCS and recovered after few minutes through a recovery port placed diametrically opposite to the injection site (fig. 5f). An excess amount of saline was pushed through the first needle, and effluent containing the cells was collected through the recovery port. The tagged cells from the collected samples show 99% viability, indicating that force of injection and transit through the SCS does not appreciably affect cell survival (fig. 5g-i).

*i*2T2 can target SCS *in vivo* with minimal tissue trauma

Three Dutch belted rabbits injected with *i*2T2 in both eyes were sacrificed immediately following the SCS injection to evaluate device performance and its acute impact. Each injection lasted less than 20s, and a 15s delay in removing the needle avoided reflux along the needle track. None of the injections showed any visible signs of hemorrhage during the procedure. Three eyes, one from each animal, that were cut open immediately, showed a clear vitreous (absence of green dye or blood) indicating the dye was delivered within the tissue layers as expected and the injection did not cause vitreous hemorrhage. Photographs of frozen section (fig. 5j) and microCT image (fig. 5k) of the other three frozen eyes confirm these results. All three of the imaged eyes showed the contrast agent distributed through the SCS and one of the three eyes showed partial leakage of the dye into vitreous. The largest volume proven safe in our *ex vivo* experiments, 100 μl, was used for these *in vivo* injections to maximize sensitivity of visualization which is significantly higher than previously reported safe injection volumes[22,23,25]. Such large volumes (⩾100 μl) have known to cause adverse events such as backflow from needle entry, localized serous retinal elevation, or choroidal hemorrhage away from needle entry[27]. We did not see these adverse events with *i*2T2 and the injected dye travelled through SCS to reach back of the eye. Up to 100% SCS coverage observed *in vivo* (fig. 5l) immediately after injection shows that therapeutic agents can be delivered to the entire posterior section with a single minimally invasive local injection.

Macroscopic applications of *i*2T2

The basic principle of *i*2T2 can be used for multiple applications where one needs to blindly access a target tissue/cavity hiding beneath a relatively denser tissue (supplementary table-1).

Epidural injections are widely used to deliver medication into the outermost space around spinal cord (i.e. epidural space) for temporary or prolonged relief from pain or inflammation. Every injection involves a risk of injury to the dura protecting the spinal cord (and leaking of cerebrospinal fluid). Figure 6 (a-d) shows the injection into the spinal canal (porcine tissue, ex vivo) with the *i*2T2. The spinal cord was removed to enable direct visualization of the potential needle overshoot and the spinal canal (fig 6a). The *i*2T2 design depicted in fig. 1g comprises of a 18G X 9 cm needle. As the plunger was pushed forward by the operator, the needle traveled through the dense tissue in between two vertebrae and delivered the dye into the spinal canal evident by the stream of fluid and overflowing blue

dye (fig. 6b). The needle overshoot was too small to be detected (fig 6c) during fluid delivery. The needle position was subsequently confirmed by pushing the needle forward by 5 mm (fig. 6d).

Subcutaneous injections are frequently administered for medications that require slow, sustained rate of absorption. Misplaced delivery to intradermal or intramuscular locations directly affects the absorption rate which is critical for life sustaining medication like insulin for diabetic patients. The difference in resistance to fluid flow offered by the cutis and the hypodermis can be leveraged by *i*2T2 to deliver the medication subcutaneously. The operator does not need to control the needle depth to ensure delivery to the hypodermis. Figure 6 (e-h) shows subcutaneous injection (porcine tissue, ex vivo) with an *i*2T2 (design depicted in fig. 1g, 25G needle). Multiple tissue layers (dermis, hypodermis, muscle) are visible in the cross-section (fig. 6e). The needle is pre-inserted into the dermis (fig 6f) and the plunger is pushed forward. Initially the needle squeezes the tissue as it advances through the dermis and delivers the fluid immediately, as it senses reduction in resistance to fluid flow into the subcutaneous space (fig. 6g-h).

Blind insertion of a sharp needle or a trocar into the intraperitoneal space through the abdominal wall is the first step performed in every laparoscopic surgery with an inherent risk of injury to internal organs. To enable the travel of *i*2T2 through the multiple tissue layers of the abdominal wall (skin, fat, muscle, and connective tissue), we used a hydrogel plug (placed at the end of the needle tip) to avoid fluid leakage into porous tissue like muscle and fat (fig. 6i). This increased the driving force in stage-II while maintaining the force-structure in stage-III (supp. S1, fig. 6j). Figure 6 k-n and supplementary video-1 show delivery of fluid through the abdominal wall (porcine tissue, ex vivo) into a cavity below. The small hydrogel plug (2 mm long) in the needle escapes into the cavity (fig. 6m) to clear the path for the fluid as soon as the needle enters the cavity and the drop in internal pressure arrests the needle motion (fig. 6n). Similarly, the hydrogel enhanced *i*2T2 can be used to access the ventricular cavity through heart wall (supplementary video-2).

Discussion

The century-old method of injection with a hypodermic needle and a syringe is simple and effective but limited by its dependence on the operator to target the injection site. The manual feedback-based injection has prevailed despite availability of live imaging methods, largely because of its simplicity and cost-effectiveness. The intelligent-injector for tissue-targeting (*i*2T2) introduced here can deliver the same simplicity and cost-effectiveness with the precision to target the potential space of SCS between the thin tissue layers of the sclera and the choroid. This completely mechanical system, designed with simplicity being the modus operandi, can sense when the needle reaches a cavity, stop advancing, and start ejecting its payload in the target space.

Ex vivo and *in vivo* studies prove that the *i*2T2 can reliably inject in SCS to cover its large portion. Interestingly, *in vivo* injections show a better SCS coverage (up to 100%) than *ex vivo* rabbit eyes (up to 80%) for the same dosage. Porosity of the outer choroid[41] may have allowed for the fluid to spread along the periphery more easily compared to an *ex vivo*

sample that may have compromised porosity due to the loss of interstitial pressure. Minor serous choroidal detachment was observed in one of the eyes, possibly due to the large volume of injected fluid. Such small choroidal detachments often heal on their own in a few days and their occurrence can be minimized by optimizing the injected fluid volume. Unaffected by anatomical variations, *i*2T2 can be used as a universal device for SCS injection across the entire patient population. The ability to deliver and distribute live cells to the entire SCS can accelerate efforts in implementing cell therapy for curing ocular diseases[39,40].

The current design of the device leaves a small amount of dead volume which depends on the final positions of the needle-plunger and pushing-plunger. This variation in dosage due to the unknown travel distance of the needle can be minimized by reducing the diameter of the needle-plunger. Particularly, for SCS injections (100 μl) in rabbit eyes, we reduced the dead volume and its variation, from 11±8 μl to 6±4 μl, by reducing the plunger diameter from 4.78 mm to 3.25 mm. For larger dosage volumes (300 μl) the relative error can reduce further from 6% to 1.67% (Supplementary information S5). These error values are within the acceptable range for intraocular injections[42,43]. Alternatively, one could control the delivered dose by continuously monitoring the positions of the two plungers and stop injecting at a predetermined relative position of plungers to inject a known amount of dose.

The simplicity of the *i*2T2 mechanism enables its adaptation for multiple clinical indications, each with distinct design criteria. Here we focused on the ocular applications of the *i*2T2 and demonstrated its ability to target a micron-thin cavity below a millimeter-thin tissue. Preliminary ex vivo experiments for epidural injection, subcutaneous delivery and peritoneal access demonstrated the versatility and adaptability of the *i*2T2. Currently, such cavities are accessed either blindly with prior knowledge of the anatomy through imaging, or with the help of live imaging systems[6] like fluoroscopy[7], CT scan[8] or ultrasound[9,10]. Performing a blind injection is simplest, but carries the risk of missing the target and damaging vital organs in the vicinity. Procedures to access these cavities could benefit from the *i*2T2 mechanism. For instance, in case of venipuncture for intravenous injection or fluid administration, one could use *i*2T2 to target the right depth. Combined with vein-illumination technology such as VeinViewer™, one can imagine near perfect venous access, reducing complications and ensuring vein preservation[44]. A spring-loaded/hydraulic-powered pushing-plunger can automate the *i*2T2 for more complex procedures and robotic systems. The design process and the analytical model can enable quick iterations for new applications.

In summary, we have introduced a generalized *i*2T2 mechanism for targeted needle insertion, and shown its application for targeting the SCS. This mechanical system senses when the needle reaches the target cavity and immediately stops advancing, while injecting its payload of therapeutic agent or live cells. *i*2T2 enables drug delivery to the entire posterior eye through SCS despite anatomical variation within patient population which could help address multiple debilitating ocular diseases including uveitis, diabetic retinopathy, and macular degeneration. The simplicity and versatility of *i*2T2 allows one to adapt the design for multiple clinical applications and offers an automated approach to access the targeted tissue or cavity through an overlaying tissue layer. This cost-effective,

sensitive, and user-friendly technology enables the next generation of precisely targeted safer injections.

Methods

Device fabrication:

Standard hypodermic needle and components of commercially-available plastic syringes were used to fabricate functional prototypes. Two standard syringes are required to make one *i*2T2. First, the barrel of one syringe is cut to remove the front end that mounts the needle. Next, the plunger from the second syringe is machined to create a needle-plunger and inserted into the machined barrel. A needle-plunger-seat (to prevent backward motion during pre-insertion) is created by inserting a metal wire (stainless steel 316L, diameter: 300 μm) across the barrel such that wire is affixed to the barrel wall. Finally, a commercially available standard hypodermic needle is mounted on the Luer lock connector of the needle-plunger. These process steps can be applied to any syringe to make a *i*2T2 device and any commercially available hypodermic needle with a Luer lock connector can be mounted on it. Other design variations were also prototyped similarly using off-the-shelf components to create *i*2T2. The design used for ocular drug delivery uses fluidic connector which acts as the needle-plunger-seat eliminating the need for metal wire and the needle (30G) is mounted directly on the needle plunger using epoxy adhesive.

Force measurements:

All the measurements were performed using a Universal testing machine by ADMET. To measure the driving force in stage II, needle was inserted into the tissue to bury the tip and fluidic pressure was applied using a pushing plunger. Maximum force applied before there was backflow along the shaft of the needle or the fluid started infusing into the tissue was noted. Frictional force was measured separately and subtracted from the maximum applied force to calculate the driving force for each needle in stage II. For stage III driving force, needle tip was kept in open air to mimic its presence in cavity and plunger was pushed at a given rate while monitoring the maximum applied force. Similar to stage II, pushing plunger friction was subtracted to calculate stage III driving force. Opposing force for stage II was calculated by addition of needle-plunger friction and needle penetration force through the tissue. For stage III opposing force is same as the needle plunger friction (and therefore it is also independent of the needle size and plunger speed). Please refer supplementary information S1 for more details.

Ex vivo SCS injections:

Fresh bovine and porcine eyes were procured on the day of sacrifice through a local supplier (Research 87 Inc.). Fresh rabbit eyes were obtained from Pel-Freeze biologicals which were received within 48 hours of sacrifice. Eyes were stored in a refrigerator and used within 2–3 days of procurement. Eyes were secured with one hand and injections were performed with the other. The needle was oriented at an 30° angle to the sclera, with the open side of the bevel pointing towards the eye for easier pre-insertion. The needle was inserted into the sclera at a set distance from the limbus depending on the species (Bovine: 8 mm, Porcine: 5 mm, Rabbit: 3 mm). Although the needle insertion depth could exceed the scleral thickness

(measured normal to the eye surface), this angled approach ensured that the needle tip would insert completely and not leak, yet not overshoot the SCS. Multiple payloads including PBS, Green histology dye (Davidson marking system), polymer particles (Polybeads®, 0.20 μm, Polysciences Inc), and MSCs (tagged with DiD, ThermoFisher) were injected using this injection method.

Ex vivo epidural injection:

Fresh porcine back tissue with an intact spinal canal with skin was procured from a local supplier (Research 87 Inc.) and used within 12 hours of sacrifice. Blue food grade dye was used to color the injected PBS. The tissue was placed in a tray on the experimental bench with the spinal canal parallel to the table and the back skin facing the operator. The needle (18G, 9 cm long) was preinserted (5 mm deep) at an angle in between two vertebrae with the needle tip pointing towards the intervertebral space. The plunger was pushed by the operator in one continuous motion to drive the needle through the tissue and deliver the fluid into the canal without any measurable overshoot.

Ex vivo subcutaneous injection:

Fresh porcine skin with connected muscular layer was procured from a local supplier (Research 87 Inc.) and used within 12 hours of sacrifice. Blue food grade dye was used to color the injected PBS. The tissue was placed in a tray on the experimental bench with skin facing the operator. The needle (25G, 1 in) was preinserted into the tissue to block the needle tip. The plunger was pushed by the operator in one continuous motion to drive the needle through the skin layer and deliver the fluid subcutaneously.

Ex vivo peritoneal injection:

Fresh porcine abdominal wall (full thickness) was procured from a local supplier (Research 87 Inc.) and used within 12 hours of sacrifice. Green histology dye (Davidson marking system) was used to color the injected PBS. The tissue was placed on a 4-well plate to create a cavity under the tissue with skin facing the operator. The *i*2T2 was filled with the fluid and needle was impregnated with a hydrogel plug (pre-molded to shape, agarose, 1.5%). The needle (18G, 9 cm long) was preinserted (5 mm deep) into the tissue skin to block the needle tip. The plunger was pushed by the operator in one continuous motion to drive the needle through the multiple tissue layers and deliver the fluid into the cavity under the abdominal wall.

Histology:

The eyes injected with dye were snap frozen immediately after injection by dipping the eyes into acetone maintained at (−80 ºC) on dry ice for 15 min to keep the dye from diffusing into surrounding tissue. These frozen samples were cut into smaller sections, embedded in OCT and sectioned using a cryotome (8 μm thick sections). The eyes injected with particles followed a separate protocol. Since polymeric particle do not diffuse through the tissue we fixed the whole eye by immersing it in Davidson's solution (30 ml of 95% ethyl alcohol, 20 ml of 10% neutral buffered formalin, 10 ml of Glacial Acetic Acid, 30 ml of Distilled water) for 12 hours. Then the samples were transferred into graded ethanol series (70% to 80% to

90% to 100%) for one day each. Finally, paraffin blocks were prepared from fixed tissue and sectioned at 5 μm thickness. This protocol was also effective for serial sectioning. All the sectioned were stained with hematoxylin and eosin.

MicroCT:

We used The Nikon Metrology (X-Tek) HMXST225 MicroCT system to perform three-dimensional imaging of the injected contrast agent. The eyes were frozen immediately after injection and imaged in frozen condition. Scan time was limited to 15 minutes to avoid melting of the sample during imaging. The raw image data was processed using VGStudio MAX software and 40–60 μm thick sections were obtained. For the experiment with diffusion of the contrast agent, the eye was maintained at room temperature.

SCS coverage measurement:

CAD files were generated for the injected contrast agent and the posterior section of the eye based on the 3-dimentional image constructed by imaging with mictoCT system. Intensity cut-off was manually adjusted to extract dye or eye portion. Total available SCS are was assumed to be same as the inner surface area of the sclera in posterior section. Area of the 3D model was quantified with a CAD software (CATIA™). Relative SCS coverage was calculated by dividing the dye area with total available SCS area.

Cell injection and sample recovery:

MSCs were cultured under standard media conditions. Prior to injection, cells were stained with a cell dye (DiD or CellTrace Violet). Stained cells (1 million) were injected into the SCS using *i*2T2 and recovered after few minutes through a recovery port placed diametrically opposite to the injection site (fig. 5d). An excess amount of saline was pushed through the first needle, and effluent containing the cells was collected through the recovery port. Collected samples were pooled together and analyzed with a flow cytometer.

In vivo studies:

Ethical approval was given by the Institutional Animal Care and Use Committee of Schepens Eye Research Institute (Boston, USA). All animals were treated according to guidelines of the Association for Research in Vision and Ophthalmology Statement for the Use of Animals in Ophthalmic and Vision Research. Three Dutch Belted rabbits (2–3 kg body weight) were anesthetized with intramuscular injection of ketamine hydrochloride (35 mg/kg) and xylazine hydrochloride (5 mg/kg), and topical administration of 0.5% proparacaine. The needle of *i*2T2 was inserted in the superior temporal quadrant at a 30° angle (similar to ex vivo injection) through the conjunctiva into the sclera, 3 mm posterior from the limbus, with the bevel facing downward. We injected 100 μl mixture of green histology dye (Davidson Marking System) and contrast agent (Ultravist-370 diluted 1:1 with PBS) in six eyes within 15–20 s each. To avoid excessive reflux, the injection was followed by a 15 s delay before removing the needle from the eye. Animals were sacrificed immediately after SCS injection by a lethal dose of pentobarbital (100mg/kg) injected intravenously. After euthanizing and enucleation, one eye from each animal was opened immediately to observe whether the injected fluid was delivered intra-vitreally, while the

other eye was enucleated and snap frozen for further analysis (microCT imaging and cryosectioning).

Data availability

The authors declare that all data supporting the findings of this study are available within the paper and its supplementary information.

Supplementary Material

Refer to Web version on PubMed Central for supplementary material.

Acknowledgements

Funding for this research was provided by the R01HL095722 to JMK. Animal experiments were funded through Boston-KPro research fund to MGA and A.C. We would like to thank Dr. Yookyung Jung and Prof. Charles P. Lin for the use of intravital microscope, H. Greg Lin and Harvard's Center for Nanoscale Systems for use of microCT system, and Kathleen Cormier and the Hope Babette Tang Histology Facility at the Koch Institute at MIT for performing histology sections. We also thank the Schepens Eye Research Institutés Animal Facility, specially, Jessica Hoadley, Marie Ortega and Candace Beiler for their help. We greatly appreciate the feedback on performing SCS injections with *i*2T2 from Dr. Demetrios Vavvas, Dr. Vannarut Satitpitakul, and Dr. Kunal Suri from Massachusetts eye and ear infirmary (MEEI).

References:

1. Tsukuda Y et al. Venipuncture Nerve Injuries in the Upper Extremity From More Than 1 Million Procedures. J. Patient Saf. (2016).
2. Oven S & Johnson J Radial Nerve Injury after Venipuncture. J. Hand Microsurg 9, 043–044 (2017).
3. Aders A & Aders H Anaesthetic adverse incident reports: an Australian study of 1,231 outcomes. Anaesth. Intensive Care 33, 336–44 (2005). [PubMed: 15973916]
4. Fuller J, Scott W, Ashar B & Corrado J Laparoscopic Trocar Injuries: A report from a U.S. Food and Drug Administration (FDA) Center for Devices and Radiological Health (CDRH) Systematic Technology Assessment of Medical Products (STAMP) Committee: FDA Safety Communication. (2003). at <http://www.fda.gov/MedicalDevices/Safety/AlertsandNotices/ucm197339.htm>
5. Benzon HT, Huntoon MA & Rathmell JP Improving the Safety of Epidural Steroid Injections. JAMA 313, 1713 (2015). [PubMed: 25822848]
6. Wu T, Zhao W, Dong Y, Song H & Li J Effectiveness of Ultrasound-Guided Versus Fluoroscopy or Computed Tomography Scanning Guidance in Lumbar Facet Joint Injections in Adults With Facet Joint Syndrome: A Meta-Analysis of Controlled Trials. Arch. Phys. Med. Rehabil 97, 1558–1563 (2016). [PubMed: 26705882]
7. Evansa I, Logina I, Vanags I & Borgeat A Ultrasound versus fluoroscopic-guided epidural steroid injections in patients with degenerative spinal diseases. Eur. J. Anaesthesiol 32, 262–268 (2015). [PubMed: 24841502]
8. Bui J & Bogduk N A Systematic Review of the Effectiveness of CT-Guided, Lumbar Transforaminal Injection of Steroids. Pain Med 14, 1860–1865 (2013). [PubMed: 24330228]
9. Whipple TL in Sports Injuries 2335–2342 (Springer Berlin Heidelberg, 2015). doi: 10.1007/978-3-642-36569-0_183
10. D'Agostino MA & Schmidt WA Ultrasound-guided injections in rheumatology: Actual knowledge on efficacy and procedures. Best Pract. Res. Clin. Rheumatol 27, 283–294 (2013). [PubMed: 23731936]
11. PALMER R Instrumentation et technique de la coelioscopie gynécologique. Gynecol. Obstet. (Paris). 46, 420–31 (1947). [PubMed: 18917806]
12. Bassett EK et al. Design of a mechanical clutch-based needle-insertion device. Proc. Natl. Acad. Sci. U. S. A. 106, 5540–5 (2009). [PubMed: 19307560]

13. Begg NDM Blind Transmembrane Puncture Access: Design and Development of a Novel Laparoscopic Trocar and Blade Retraction Mechanism. (2011).
14. Anderson TA, Kang JW, Gubin T, Dasari RR & So PTC Raman Spectroscopy Differentiates Each Tissue from the Skin to the Spinal Cord. Anesthesiology 125, 793–804 (2016). [PubMed: 27466032]
15. Riley ET & Carvalho B The Episure syringe: a novel loss of resistance syringe for locating the epidural space. Anesth. Analg 105, 1164–6 (2007). [PubMed: 17898406]
16. Vilos G & Vilos A The Veress needle causes most laparoscopic injuries and should be abandoned: AGAINST: Evidence indicates that the primary trocar, not the Veress, causes most serious complications. BJOG An Int. J. Obstet. Gynaecol 122, 142–142 (2015).
17. Vindal A & Lal P The Veress needle causes most laparoscopic injuries and should be abandoned: FOR: The open technique is safer and saves time. BJOG An Int. J. Obstet. Gynaecol 122, 141–141 (2015).
18. Cornette B & Berrevoet F Trocar Injuries in Laparoscopy: Techniques, Tools, and Means for Prevention. A Systematic Review of the Literature. World J. Surg 40, 2331–2341 (2016). [PubMed: 27146054]
19. Gonenc B, Taylor RH, Iordachita I, Gehlbach P & Handa J Force-sensing microneedle for assisted retinal vein cannulation in IEEE SENSORS 2014 Proceedings 698–701 (IEEE, 2014).
20. Moisseiev E, Loewenstein A & Yiu G The suprachoroidal space: From potential space to a space with potential. Clin. Ophthalmol 10, 173–178 (2016). [PubMed: 26869750]
21. Olsen TW et al. Cannulation of the Suprachoroidal Space: A Novel Drug Delivery Methodology to the Posterior Segment. Am. J. Ophthalmol 142, (2006).
22. Patel SR, Lin ASP, Edelhauser HF & Prausnitz MR Suprachoroidal drug delivery to the back of the eye using hollow microneedles. Pharm. Res 28, 166–76 (2011). [PubMed: 20857178]
23. Patel SR et al. Targeted administration into the suprachoroidal space using a microneedle for drug delivery to the posterior segment of the eye. Investig. Ophthalmol. Vis. Sci 53, 4433–4441 (2012). [PubMed: 22669719]
24. Abarca EM, Salmon JH & Gilger BC Effect of choroidal perfusion on ocular tissue distribution after intravitreal or suprachoroidal injection in an arterially perfused ex vivo pig eye model. J. Ocul. Pharmacol. Ther 29, 715–22 (2013). [PubMed: 23822159]
25. Kadam RS, Williams J, Tyagi P, Edelhauser HF & Kompella UB Suprachoroidal delivery in a rabbit ex vivo eye model: influence of drug properties, regional differences in delivery, and comparison with intravitreal and intracameral routes. Mol. Vis 19, 1198–210 (2013). [PubMed: 23734089]
26. Gilger BC, Abarca EM, Salmon JH & Patel S Treatment of acute posterior uveitis in a porcine model by injection of triamcinolone acetonide into the suprachoroidal space using microneedles. Investig. Ophthalmol. Vis. Sci 54, 2483–2492 (2013). [PubMed: 23532526]
27. Chen M, Li X, Liu J, Han Y & Cheng L Safety and pharmacodynamics of suprachoroidal injection of triamcinolone acetonide as a controlled ocular drug release model. J. Control. Release 203, 109–117 (2015). [PubMed: 25700623]
28. Chiang B et al. Thickness and Closure Kinetics of the Suprachoroidal Space Following Microneedle Injection of Liquid Formulations. Investig. Opthalmology Vis. Sci 58, 555 (2017).
29. Chiang B, Venugopal N, Edelhauser HF & Prausnitz MR Distribution of particles, small molecules and polymeric formulation excipients in the suprachoroidal space after microneedle injection. Exp. Eye Res 153, 101–109 (2016). [PubMed: 27742547]
30. Gu B et al. Real-Time Monitoring of Suprachoroidal Space (SCS) Following SCS Injection Using Ultra-High Resolution Optical Coherence Tomography in Guinea Pig Eyes. Invest. Ophthalmol. Vis. Sci 56, 3623–34 (2015). [PubMed: 26047049]
31. Prevalence of Adult Vision Impairment and Age-Related Eye Diseases in America (Based on 2010 U.S. Census populations). at <https://www.nei.nih.gov/eyedata/adultvision_usa>
32. Projections for AMD (2010–2030-2050) based on 2010 U.S. Census populations. at <https://www.nei.nih.gov/eyedata/amd#5>
33. Projections for Diabetic Retinopathy (2010–2030-2050) Based on 2010 U.S. Census populations. at <https://www.nei.nih.gov/eyedata/diabetic#5>

34. Chen K, Rowley AP, Weiland JD & Humayun MS Elastic properties of human posterior eye. J. Biomed. Mater. Res. - Part A 102, 2001–2007 (2014).
35. Peden MC et al. Ab-externo AAV-mediated gene delivery to the suprachoroidal space using a 250 micron flexible microcatheter. PLoS One 6, (2011).
36. Norman RE et al. Dimensions of the human sclera: Thickness measurement and regional changes with axial length. Exp. Eye Res 90, 277–284 (2010). [PubMed: 19900442]
37. Vurgese S, Panda-Jonas S & Jonas JB Scleral thickness in human eyes. PLoS One 7, (2012).
38. Goldstein D a. Achieving Drug Delivery Via the Suprachoroidal Space. Retina Today 82–84 (2014).
39. Zhang L et al. Long-Term Therapeutic Effects of Mesenchymal Stem Cells Compared to Dexamethasone on Recurrent Experimental Autoimmune Uveitis of Rats. Investig. Opthalmology Vis. Sci 55, 5561 (2014).
40. Cao J et al. Human umbilical tissue-derived cells rescue retinal pigment epithelium dysfunction in retinal degeneration. Stem Cells 34, 367–379 (2016). [PubMed: 26523756]
41. Nickla DL & Wallman J The multifunctional choroid. Prog. Retin. Eye Res 29, 144–168 (2010). [PubMed: 20044062]
42. Raju JR & Weinberg DV Accuracy and precision of intraocular injection volume. Am. J. Ophthalmol 133, 564–6 (2002). [PubMed: 11931796]
43. Muffly MK et al. Small-Volume Injections: Evaluation of Volume Administration Deviation From Intended Injection Volumes. Anesth. Analg 125, 1192–1199 (2017). [PubMed: 28338490]
44. Strehle E-M Making the invisible visible: near-infrared spectroscopy and phlebotomy in children. Telemed. J. E. Health. 16, 889–93 (2010). [PubMed: 20925568]

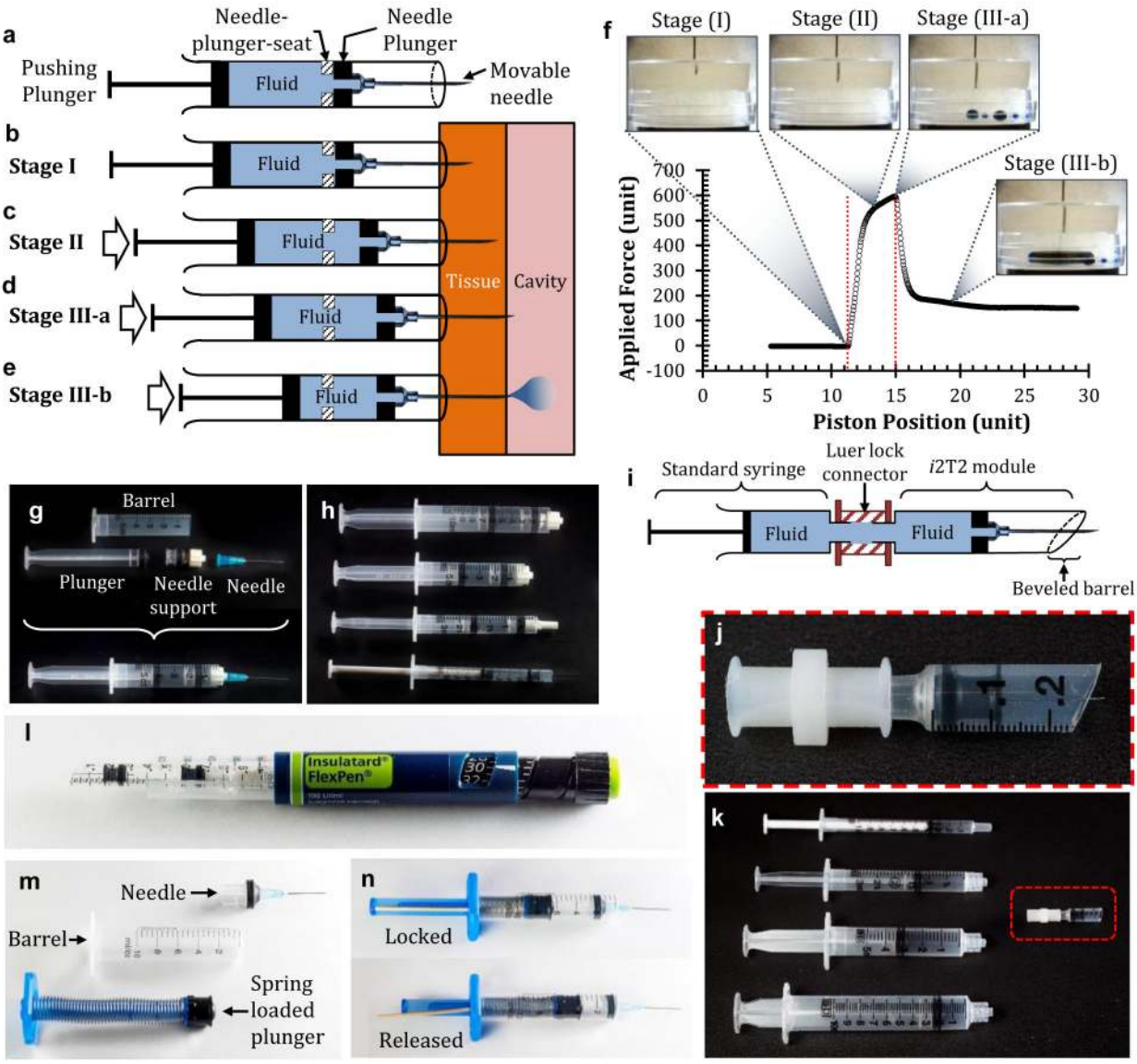

Figure 1:

The *i*2T2 design and its mechanism of action. (a) Schematic diagram of *i*2T2 with its critical components i.e. pushing plunger, needle plunger, mechanical stop, fluid, and needle (b-e) The working mechanism of the *i*2T2 as the needle moves through the tissue wall (f) Position of the needle tip and corresponding force applied on the plunger (g) Assembled and separated components of the *i*2T2 (h) The *i*2T2 fabricated with multiple type of syringes (1 ml, 3 ml, 5 ml, and 10 ml). (i-k) Design variation to enable direct use of a commercial syringe with *i*2T2 module (l) *i*2T2 adapted to fit an insulin injector (m) Components of a spring-loaded *i*2T2 (n) The pushing plunger is locked mechanically to prevent unwanted motion of the plunger. When the lock is released, the plunger is pushed forward.

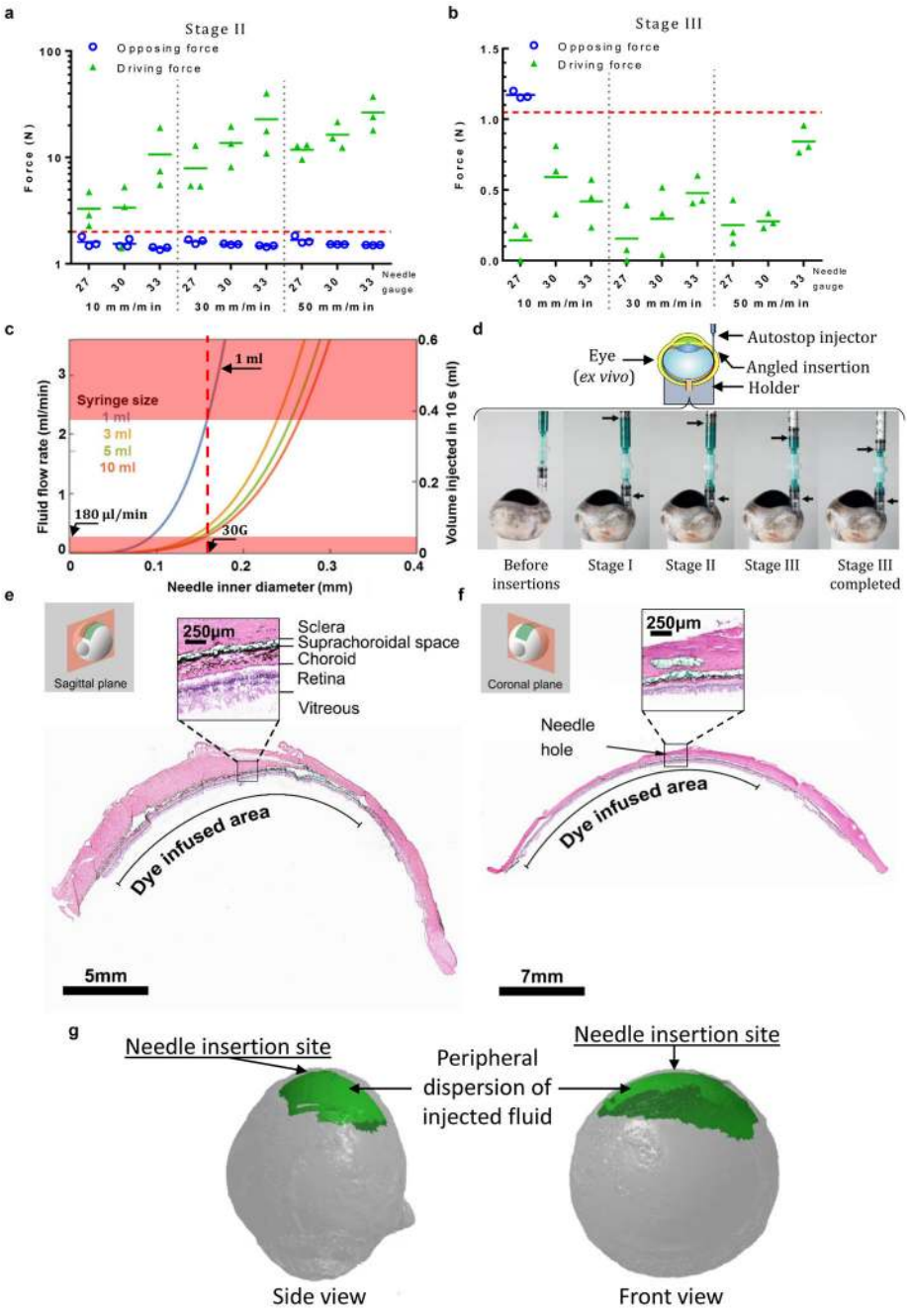

Figure 2.

The *i*2T2 can inject into the SCS to deliver drug to the back of the eye (a) driving and opposing forces measured in sclera for stage II (b) driving and opposing forces in stage III (c) model predicting the flow-rates that allows for automatic stop for a range of needles and syringes helps with design of *i*2T2 for SCS injection (d) SCS injection with the *i*2T2 showing the angle of insertion and position of plungers in different stages (e-f) Histology images of the injected eyes show the presence of green dye in the SCS. (g) 3D reconstructions of microCT imaged eyes following injection with contrast agent. The experiments were repeated independently (n>10) with similar results shown in (e-g).

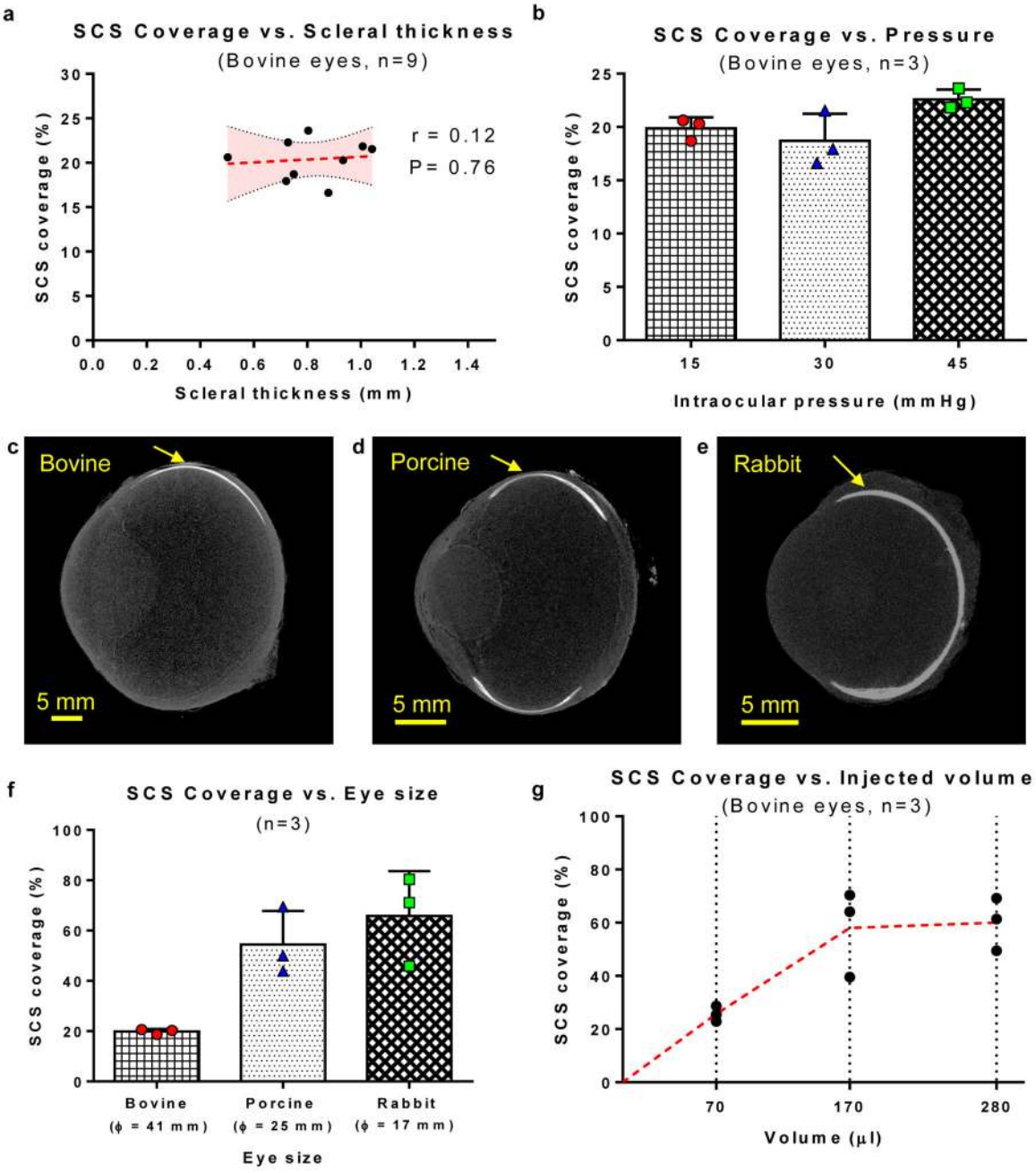

Figure 3:

*i*2T2 can inject into the SCS and achieve large coverage despite anatomical variations (a) SCS coverage for injections performed with *i*2T2 is not influenced by variations in scleral thickness (Dotted red line indicates linear regression fit and shaded region shows 95% confidence interval. Pearson's r test indicates non-significant correlation with P=0.76) (b) SCS coverage for injections performed with *i*2T2 is not influenced by variations in intraocular pressure. (Test: Ordinary one-way ANOVA) (c-e) MicroCT images of bovine, porcine, and rabbit eyes injected with contrast agent. Arrow indicates the location of injection. The experiments were repeated independently (n=3) with similar results. (f) For a

given volume of injection (120 μl) ocular coverage increases for smaller eye size (Error bars indicate standard deviation). (g) SCS coverage can be improved by increasing the amount of fluid injected into the SCS (red dotted line indicates the line connecting mean values).

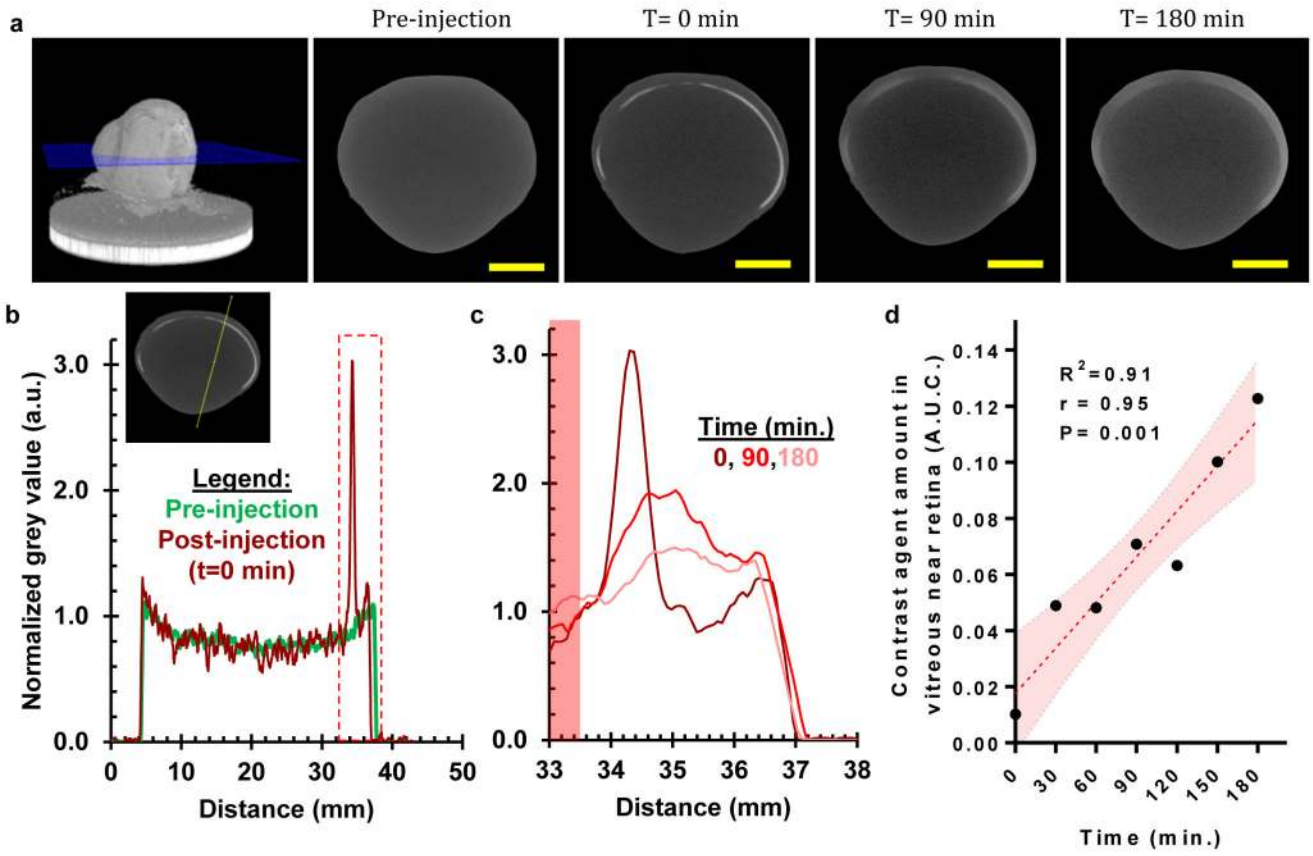

Figure 4:

Drug injected into the SCS with the *i*2T2 can reach the inner tissue layers of the retina and choroid through diffusion shortly after injection (a) MicroCT images show that the contrast agent (Iopromide, MW:791) injected in SCS diffuses into surrounding tissue over time (scale bar: 10 mm, The experiments were repeated independently (n=2) with similar results. (b) Normalized grey value, indicative of the concentration of contrast agent, is high in the SCS where the contrast agent was injected. The inset shows a representative cross-section showing the line where mean grey value was measured (c) A closer look at the tissues of interest (vitreous near retina, retina, choroid, and posterior sclera) shows the contrast agent diffusing in surrounding tissue layers over time (not all data points shown for clarity) (d) Increasing amount of drug (as represented by A.U.C.) in vitreous region near retina (highlighted with red area in inset-5c) indicates diffusion of the injected molecule into the vitreous through multiple tissue layers including the retina and Bruch's membrane. (The red dotted line indicates linear fit and the shaded region shows 95% confidence interval. Pearson's r test indicates significant correlation with r=0.95 and P=0.001).

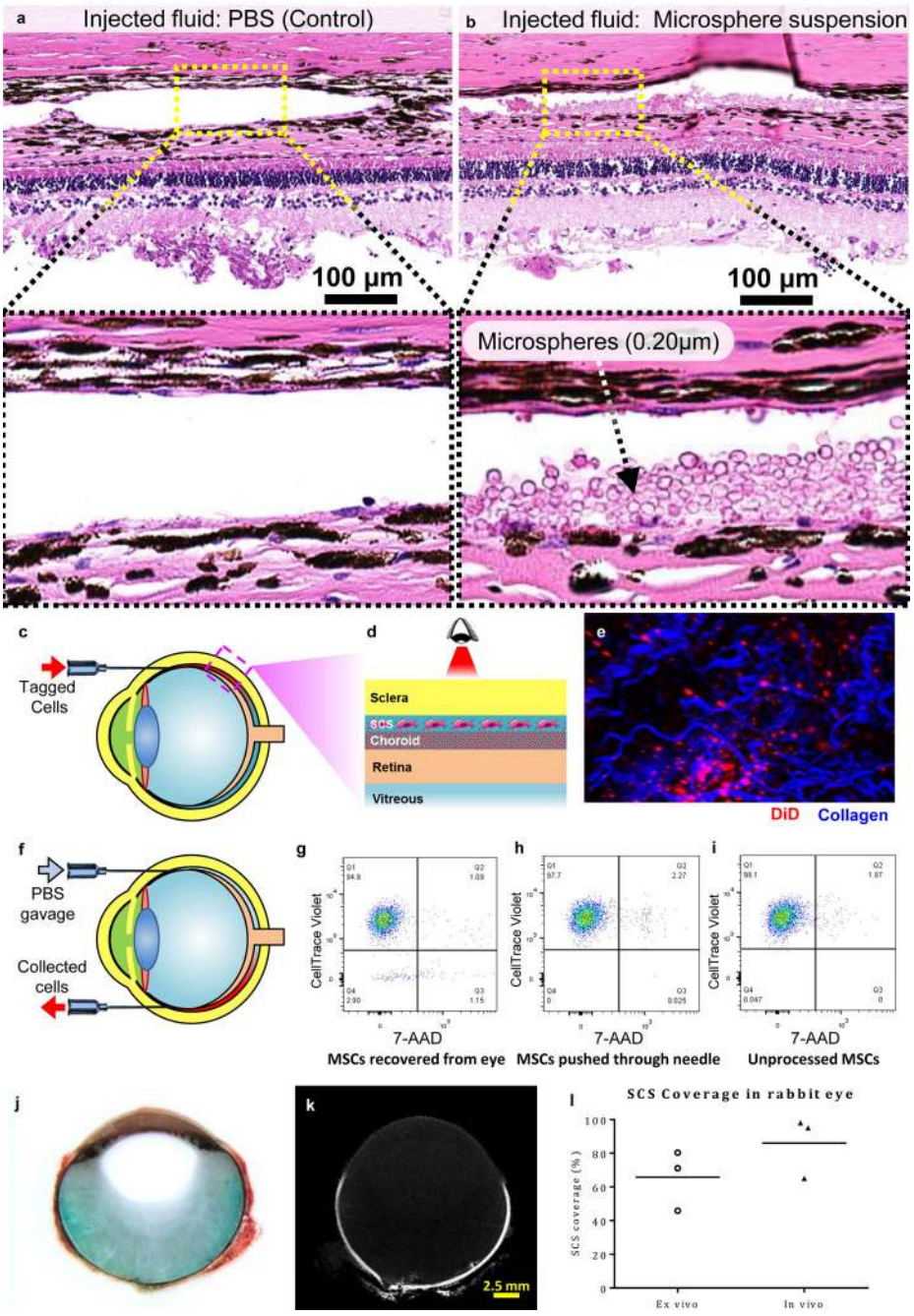

Figure 5:

The *l*2T2 can be used to deliver micro-particles and cells throughout the entire SCS. (a) PBS injected into SCS as a control. (b) polymer micro-particles delivered into SCS. (c) DiD tagged cells (red) delivered via SCS injection can be (d) visualized with (e) intravital imaging. (Collagen fibers were detected as second harmonic generations shown in blue.) (f) immediate retrieval of the injected cells (g-i) Dot plots from FACS analysis indicate 99% viability of the retrieved cells in samples after delivery through the needle and recovery from the SCS, which was similar to control cells that were not passed through the SCS (~99%). Lower quadrants show unstained cells. (samples from multiple (n=3) independent

experiments were combined together to reach minimum cell number threshold for the cytometer) (j-l) *In vivo* SCS injections in rabbits show that a large area is covered with a single injection containing a mixture of green dye and microCT contrast agent. (j) Photograph of a rabbit eye embedded in OCT and sectioned after *in vivo* SCS injection. Injected green dye diffuses from the periphery towards the center indicating that the retina and choroid were exposed to the dye. Red color indicates blood that is observed only outside the sclera due to enucleation of eyes. Lack of blood inside the globe indicates absence of internal hemorrhage. (k) MicroCT image of the same sample showing contrast agent (white) dispersed along the ocular periphery in the SCS (l) SCS coverage observed *in vivo* in comparison with *ex vivo* coverage in rabbit eyes. All the experiments were repeated independently (n=3) with similar results.

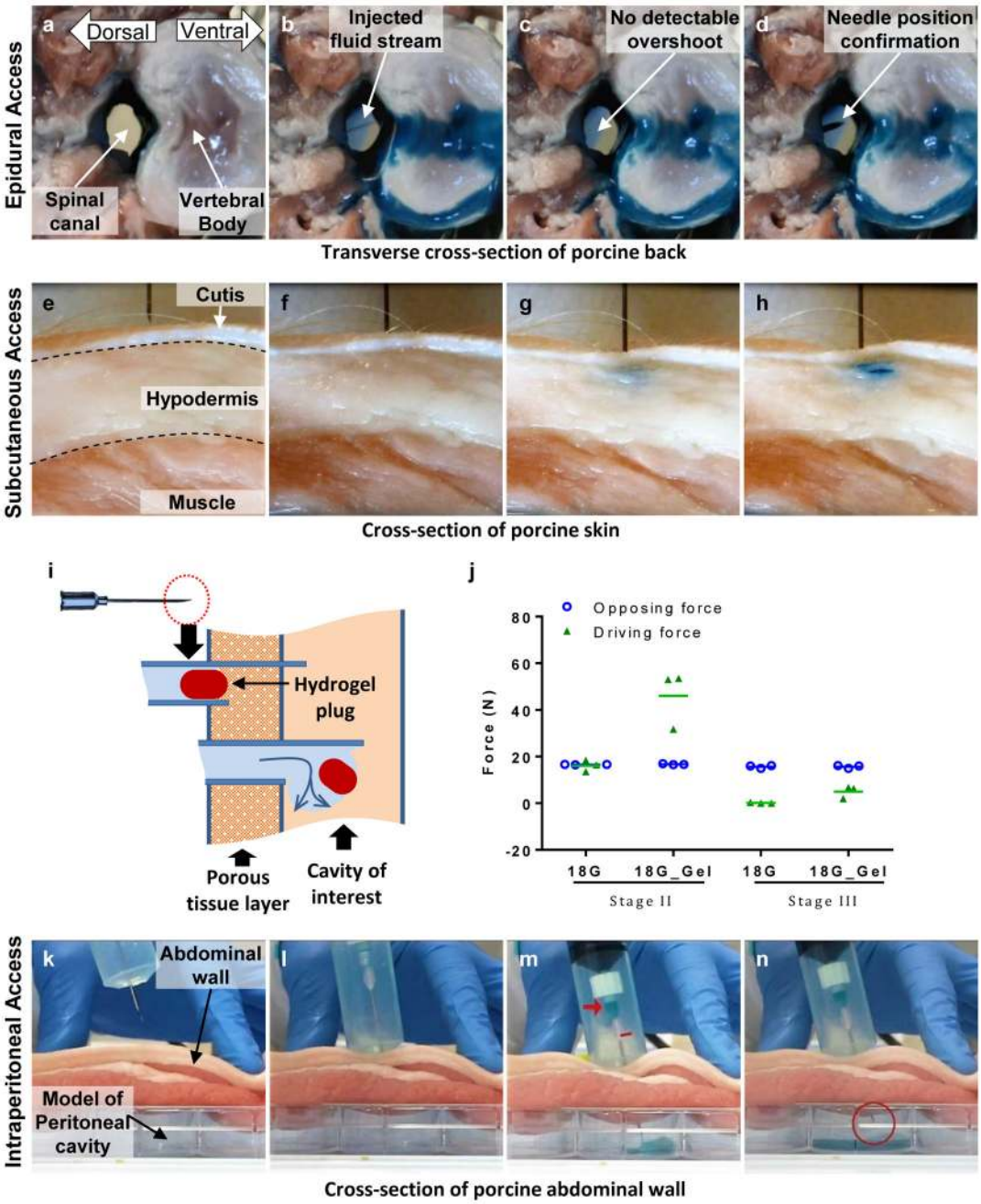

Figure 6:

Potential utility of *i*2T2 as a technology for accessing tissues and tissue compartments(a-d) Epidural access: i2T2 delivers the fluid into the spinal canal without any detectable overshoot (e-h) Subcutaneous delivery with the *i*2T2. (i) Hydrogel-plug based enhancement of *i*2T2 (j) driving forces in stage-II are improved by the hydrogel plug without affecting the force distribution in stage-III while injecting through muscle. (k-m) Intraperitoneal access with *i*2T2 enhanced with a hydrogel plug.